



Silica modification of titania nanoparticles for a dye-sensitized solar cell

Naji Al Dahoudi^{a,b,*}, Junting Xi^{a,c}, Guozhong Cao^a

^a Department of Materials Science and Engineering, University of Washington, Seattle, WA 98195, USA

^b Physics Department, Al Azhar University-Gaza, P.O. Box 1277, Gaza, Palestine

^c School of Chemistry and Chemical Engineering, Southeast University, Nanjing, Jiangsu 211189, China

ARTICLE INFO

Article history:

Received 22 July 2011

Received in revised form 3 October 2011

Accepted 4 October 2011

Available online 29 October 2011

Keywords:

Dye-sensitized solar cell

Silica modification

Titanium oxide

ABSTRACT

Nanocomposites of commercially available titanium oxide (TiO₂) nanoparticles (P25) and a silane coupling agent, methacryloxypropyltrimethoxysilane (MPTS), were incorporated into a homogeneous porous material after UV treatment and heating at 450 °C in the air. A dye-sensitized solar cell utilizing this UV-polymerized MPTS-modified sample exhibited significant enhancements in total performance when compared with an analogous cell prepared without MPTS. The photovoltaic enhancement was mainly achieved due to a significant increase in photocurrent density. This improvement is believed to be caused by the increased contact achieved between the small nanoparticles when suspended in a homogeneous, multiporous structure, which in turn would optimize the paths for electron transport. The larger surface area and pore volume resulted in an increase in the dye uptake amount and in the fast redox activity of the electrolyte, enhancing dye regeneration. Furthermore, the measured diffuse reflectance indicated greater light scattering inside the TiO₂ multiporous structure.

© 2011 Elsevier Ltd. All rights reserved.

1. Introduction

In addition to the prospect of global warming and climate change from the use of fossil fuels, one of the most critical challenges facing the world today is the global energy crisis. Seeking clean, cost-competitive, renewable energy resources is an unavoidable issue. In addition to tidal power, nuclear energy and wind energy, solar energy constitutes a strategic energy source, but its fate lies in the ability to develop and implement cost-effective solar cells. Dye-sensitized solar cells (DSCs) have been widely studied and developed after a report by Graetzel and co-workers who reported an overall energy conversion efficiency of 11% for the cells [1–3]. The benefits of DSCs are that their manufacturing process is less expensive and produces less contamination, and most of the materials used are abundant when compared with those used in commercial silicon-based solar cells.

The applicability of the DSCs is based on the electrochemical techniques utilized for the interfaces between the dye adsorbed onto a porous network of semiconducting oxides, such as TiO₂, NbO₂, and ZnO [4], and a redox electrolyte [5]. Specifically, the structure and morphology of the photoelectrode play vital roles in the development of such materials [6]. This is true because the mechanism of the DSCs is based on the dye absorption of pho-

tons from the solar spectrum, resulting in the excitation of dye molecules, which then inject electrons into a semiconducting oxide to be transported through a transparent conducting electrode via an external circuit. To regenerate the original state of the oxidized dye, electrons are received from the electrolyte redox solution. Unfortunately, conduction band electrons may also be captured by a triiodide-oxidized species of the electrolyte; this recombination is one of the drawbacks to the performance of the DSCs because it lowers the open circuit voltage (V_{OC}). The relationship between V_{OC} and the recombination rate constant (k_b) is explained by the following equation [7]:

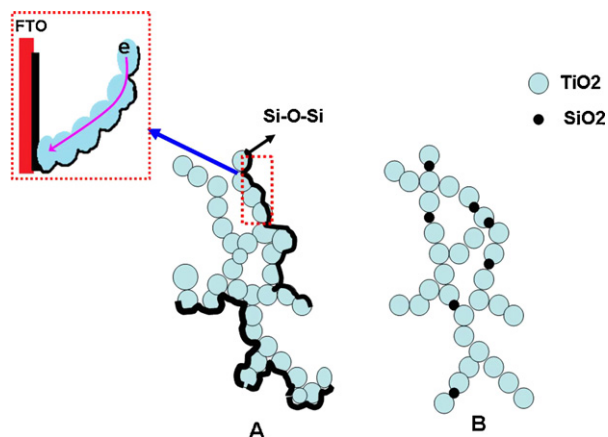
$$V_{oc} = \frac{kT}{e} \ln \left(\frac{I_{inj}}{n_{cb} k_b [I_3^-]} \right)$$

where k is the Boltzmann constant, T is the temperature, e is the electron charge, I_{inj} is the injection flux, n_{cb} is the density of electrons in the conduction band, and $[I_3^-]$ is the concentration of oxidized species. Based on this equation, it appears there are two main routes to improve the performance of the DSC. One way is to suppress recombination (the leakage current) to increase V_{OC} by constructing energy barriers at the electrode–electrolyte interface. Another route is to enhance electron transport in the electrodes by increasing the surface area of the porous photoanode with larger dye loading.

Inorganic–organic binder systems such as tetraethoxysilane (TEOS), 3-glycidoxypropyltrimethoxysilane (GPTS), or 3-methacryloxypropyltrimethoxysilane (MPTS) have also been used to enhance the electrical and mechanical properties of indium tin

* Corresponding author at: Department of Physics, Al-Azhar University- Gaza, Gaza, Palestine. Tel.: +970 599 471245.

E-mail addresses: naji@alazhar.edu.ps, dah288@yahoo.com (N.A. Dahoudi).



Scheme 1. (A) Formation of Si-O-Si network covered the TiO₂ nanoparticles. (B) Formation of SiO₂ nanoparticles in between the TiO₂ network.

oxide (ITO) nanoparticle layers [8]. These organofunctional silanes are hybrid compounds that combine the functionality of a reactive organic group with an inorganic alkyl silicate in a single molecule. These special properties mean they can be used as “molecular bridges” between inorganic materials (e.g., TiO₂ nanoparticles) and organic polymers. Additionally, silica-modified titanium dioxide has been used in photocatalysis [9–12], where the silica was utilized to increase adsorption near the active sites, which in turn increased the efficiency of the photocatalytic reactions.

Strategies for silane surface treatments depend on the number of hydroxyl groups present on the surface and their accessibility for bonding. A simple example is the reaction of organosilanes to form a monolayer, where P25 nanoparticles are silanized by the addition of a small amount of hydrolyzed MPTS. The hydrolysis of the alkoxy group results in the formation of a silanol group (R_n-Si(OH)_{4-n}), which can interact with the OH groups on the surfaces of the titania nanoparticles through hydrogen bonding (Ti-OH...HO-Si) or with another silane molecule (Si-OH...OH-Si) [13–15]. Following heat treatment, dehydration of the formed hydrogen bonds produces siloxane cross linkages between the silane and titania surface (Ti-O-Si) and forms self-assembled monolayers by the condensation of neighboring silane molecules (Si-O-Si), as shown in Scheme 1A. Interestingly, González et al. [16] prepared a closely packed, self-assembled monolayer by reacting different chain lengths of alkyltrialkoxysilanes with TiO₂ nanoparticles, which led to the formation of a densely packed alkylsiloxane network. The combustion of the organic species and cross linkage of the silane are expected to form a mesoporous structure and compact the titania nanoparticles further together, enhancing the pathway of the charge carriers across the photoanode to be collected by the working electrode. The hydrolyzed silica is also expected to enhance the adhesion of the layer on the FTO substrate, forming a very thin buffer layer and preventing further recombination of the electrons with the trap sites on the surface of the titania nanoparticles.

A proposed scenario for the formation of the silica nanoparticles on the surface of the titania nanoparticles is shown in Scheme 1B. Interestingly, the transformation from the silanol bonds into siloxane bonds is stable at higher densities of silanol bonds and at higher calcination temperatures (above 500 °C) [17]. Nur [18] prepared silica nanoparticles attached to the surface of titanium oxide nanoparticles by repeated hydrolyzes and calcinations at 550 °C, and he found that the surface attachment of titania with the silica nanoparticles enhanced the epoxidation activity of titania.

In this work, for the first time, an inorganic–organic hybrid material has been utilized to incorporate TiO₂ (P25)

nanoparticles into a mesoporous structure with a high surface area. More specifically, our focus was to see if MPTS is a good binder for DSC. To test this, an inorganic–organic matrix was polymerized using UV irradiation to encapsulate our nanoparticles, and then the inorganic–organic matrix was removed by annealing at a high temperature to create a multiporous structure. The electrochemical properties, dye loading, BET surface area and morphology of the modified and unmodified DSCs obtained were characterized, and the results were compared under the same conditions.

2. Experimental procedures

A TiO₂ paste was prepared by mixing 0.2 g of TiO₂ powder (P25, Degussa) with 0.7 g of polyethylene glycol (PEG400) and 0.3 g of ethanol using a mortar and pestle for 10 min (paste of bare P25). Next, a silica-modified paste was prepared by adding 0.075 g of hydrolyzed MPTS to the ethanol solution in the former paste (Paste MPTS/P25). The MPTS was hydrolyzed according to a previously reported method [8]. Briefly, 1.09 g of 0.1 M HCl was added slowly to 1 g of MPTS under stirring with reflux. The molar ratio of MPTS:H₂O was 1:1.5. When a clear solution was obtained, the solution was heated to 40 °C in an oil bath and stirred vigorously for 24 h. Thereafter, the solution was cooled to room temperature, and the resulting methanol from the reaction was extracted using a rotary evaporator at 40 °C and 80 mbar for 30 min.

The two types of TiO₂ paste were deposited on fluorine-doped SnO₂-(FTO)-coated glass substrates using the “doctor blade” technique to form 0.5 cm × 0.5 cm layers. The layers were dried at 100 °C for 30 min, followed by UV irradiation for 2 h using a 4 W UV Mineralight multiband lamp (UV 254/365 nm, UVGL-25). Finally, the layers were sintered at 450 °C for 1 h in the air. The obtained sintered layers had thicknesses between 12 and 14 μm.

The sintered films were all sensitized by immersing them in a 0.5 mM ruthenium-based N3 dye solution for 24 h. A Pt-coated silicon substrate was used as the counter electrode, and an iodide-based solution, consisting of 0.6 M tetra-butylammonium iodide, 0.1 M lithium iodide, 0.1 M iodine and 0.5 M 4-tert-butylpyridine in acetonitrile, was used as the liquid electrolyte.

Thermogravimetric analysis (TGA 7, Perkin-Elmer) was used to investigate the thermal behavior of the dried film as a function of the annealing temperature.

Photovoltaic properties of each solar cell were characterized using simulated AM 1.5 sunlight illumination with an output power of 100 mW/cm². An Ultraviolet Solar Simulator (Model 16S, Solar Light Co., Philadelphia, PA) with a 200-W Xenon Lamp Power Supply (Model XPS 200, Solar Light Co., Philadelphia, PA) was used as the light source, and a Semiconductor Parameter Analyzer (4155A, Hewlett-Packard, Japan) was used to measure the current and voltage.

The morphologies of the photoanode surfaces were characterized by scanning electron microscopy (SEM, JEOL JSM-7000), and the BET surface areas and pore size distributions of the layers were determined using a Brunauer–Emmett–Teller (BET, Quantachrome NOVA 4200e).

To measure the adsorbed amount of N3 dye on the bare P25 and MPTS/P25 films, the dye was desorbed by immersing the dye-sensitized films in a mixture of 0.1 M NaOH solution in water and ethanol (1:1, v/v). An ultraviolet–visible–near-infrared spectrophotometer (UV–VIS–NIR, Perkin Elmer Lambda 900) was employed to measure the dye concentrations of the desorbed-dye solutions, and the integrated sphere accessory was used to measure the diffused reflectances.

Electrochemical impedance spectroscopy (EIS) was performed using a Solartron 1287A coupling with a Solartron 1260 FRA/impedance analyzer to investigate the electronic and ionic processes in the DSCs.

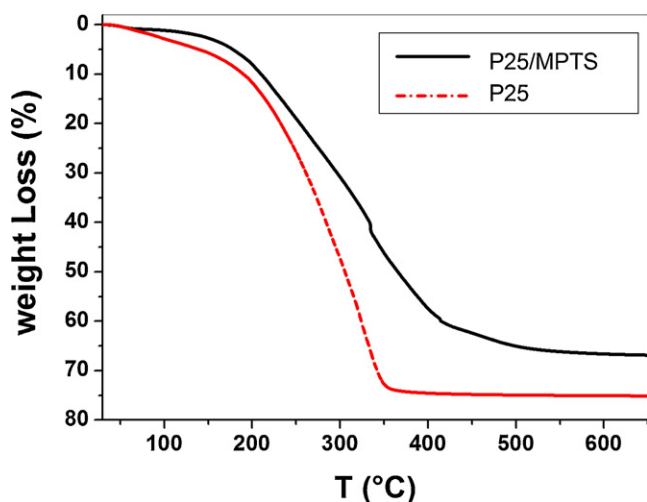


Fig. 1. TGA for bare P25 sample and MPTS modified P25 one.

3. Results and discussion

3.1. Thermal analysis

The thermal behaviors of the pure and MPTS-modified coating pastes made with redispersed P25 nanoparticles irradiated by UV-irradiation and further dried at 350 °C are shown in Fig. 1. The TG investigations were performed in the air using the same conditions as those used in layer formation. The thermogram of the bare P25 sample shows a sharp decrease in weight between 200 and 350 °C, corresponding to a weight loss of 73% due to the combustion of PEG400. A complete combustion of PEG400 is shown at 400 °C, corresponding to a 75% loss in weight, which is the concentration of the PEG400 used in the paste. Comparatively, the combustion of PEG400 is delayed in the MPTS-modified paste, due to the capping of PEG with MPTS. Only a weight loss of 46% is found at 350 °C,

and the weight continues to reduce gradually to 62% at 450 °C. This further decrease of weight at $T > 350$ °C indicates that the decompositions and combustions of the organic bonds of MPTS are not complete, where the Si–O–Si network is expected to be formed.

3.2. Surface morphology

The surface morphologies of the MPTS-modified TiO₂ nanoparticles and unmodified sample are shown in Fig. 2a and b at different magnifications. The unmodified TiO₂ nanoparticle (Fig. 2b, left) images show a cracked layer of nonhomogeneous aggregates with loose packed nanoparticles. However, the MPTS-modified sample shows a sponge-like porous structure (Fig. 2a, left) with a homogeneous distribution of closely packed, aggregated nanoparticles with well-defined morphologies within the porous structure. The UV polymerization of MPTS bound the particles, and after heating the layer, the organic species of MPTS were degraded and removed, resulting in a homogeneous multiporous structure, as shown in Fig. 2a (right). Such a structure has a higher surface roughness compared with that shown in Fig. 2b (right) and is expected to have a larger surface area, which is more convenient for electrolyte transportation and enhances the regeneration of the oxide dye, allowing for the rapid injection of a charge effectively into the photoanode.

3.3. BET surface area

The nitrogen adsorption/desorption isotherms at 77 K and the BJH pore size distributions of the MPTS/P25 and unmodified P25 samples are presented in Fig. 3a and b. Both samples have similarly shaped hysteric behaviors but have different pore volumes. The isotherm of the MPTS/P25 sample has a larger inflection for the nitrogen adsorption volume at $P/P_0 = 0.9$ than that for the unmodified sample; this result reveals the highly mesoporous nature caused by utilizing the MPTS matrix. The pore size distribution of the MPTS/P25 sample, shown in Fig. 3b, shows the multiporous structure of the film with an average diameter pore size of 4.6 nm. The unmodified sample did not show any

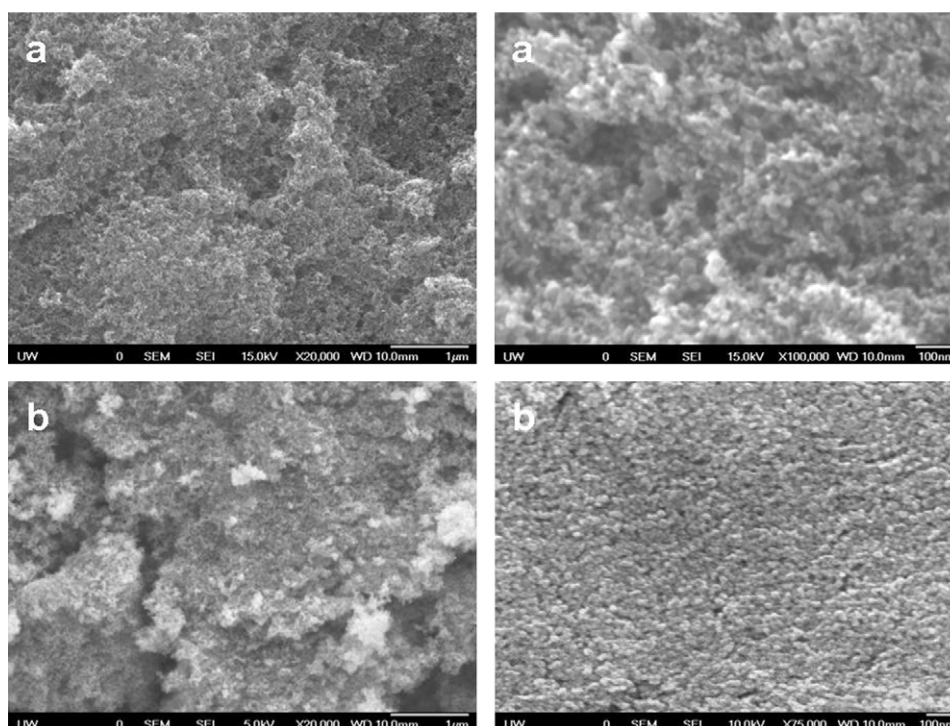


Fig. 2. SEM surface images of (a) MPTS modified TiO₂ nanoparticles and (b) unmodified TiO₂ nanoparticles electrode after UV treatment and successive heating at 450 °C.

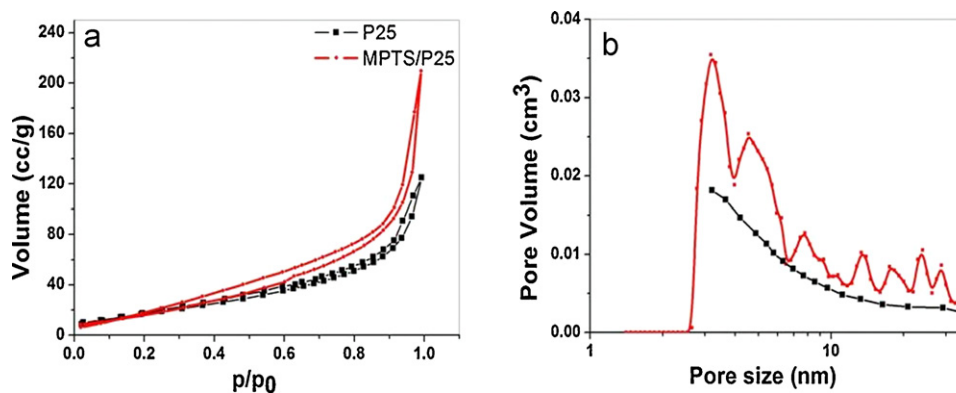


Fig. 3. (a) Adsorption-desorption isotherm using N_2 at 77K for MPTS/P25 modified and the P25 unmodified sample, and (b) represent the BJH pore size distribution for the samples in Fig. 3-a.

conformal pore size distribution greater than 3.2 nm in diameter. The determined BET surface area was found to be $92.8 \text{ m}^2/\text{g}$ for the MPTS/P25 sample, which is larger than the unmodified sample ($83 \text{ m}^2/\text{g}$). Malinowska et al. [19] reported an increase in surface area from 73 to $96 \text{ m}^2/\text{g}$ for titania and titania-silica nanoparticles, and they reported that the surface area further increases with the amount of silica added. Interestingly, a large surface area of approximately $300 \text{ m}^2/\text{g}$ was reported for a titanasilicate network using MPTS heated at 550°C after UV irradiation [20]. This larger surface area gave an explanation for the high injected photocurrent and implied that a larger exposed active region was present for the electrochemical reaction, which meant that a large amount of dye was loaded on mesoporous titania nanoparticles [21–23].

3.4. Dye loading

MPTS-modified samples offer larger surface areas for dye loading; therefore, the dye loading adsorption onto the surface of the photoanode was more readily detectable. The absorption spectra in the visible region of both the modified and unmodified samples are shown in Fig. 4. The calculated amount of dye adsorbed per unit area is $1.7 \times 10^{-7} \text{ mol}/\text{cm}^2$ for the MPTS-modified sample and $1.25 \times 10^{-7} \text{ mol}/\text{cm}^2$ for the unmodified sample. The MPTS-modified samples exhibited a larger absorption compared with the unmodified sample, which was expected as a result of the dissimilar

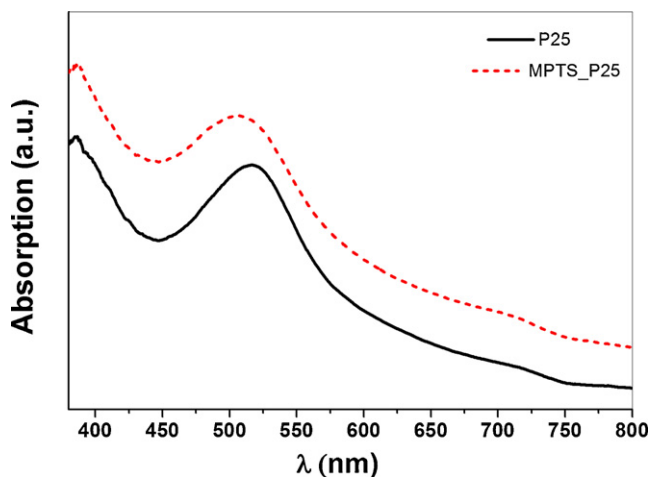


Fig. 4. The UV- VIS absorption of the detached dye from MPTS/P25 and bare P25 samples.

surface areas. Additionally, the surface roughness factors for both layers were calculated using the following equation [24]:

$$\text{SRF} = \Gamma_{\text{area}} \times N_A \times A_{\text{dye}}$$

where N_A is Avogadro's number, Γ_{area} is the number of attached dye (mol/cm^2), and A_{dye} is the surface area of the dye molecule (assumed to be 10^{-14} nm^2). By calculating the SRF for the P25 and the MPTS-modified P25, we found that the value for P25 was 752.7, while that of the MPTS-modified P25 was 1023.

3.5. EIS spectroscopy

The electrochemical reaction at the photoanode/dye/electrolyte interface is a helpful tool to understand the mechanisms of charge transport and transfer in the DSCs. The electron transport properties of the DSCs with TiO_2 electrodes made of the MPTS-modified and unmodified samples were investigated by electrochemical impedance spectroscopy (EIS), as shown in Fig. 5. After analyzing the impedance data by fitting the data with an appropriate equivalent circuit through software by Zahner, shown in Fig. 5 [25], the estimated electron transport resistance (denoted R_3) for the DSCs with MPTS/P25 was found to have a value of 90.3Ω smaller than that of the bare P25 sample with a value of 106.6Ω .

The impedance due to the electron transfer from the conduction band of the mesoscopic film to the triiodide ions in the electrolyte is represented by a semicircle in the intermediate-frequency regime [26]. The lifetime of each electron is estimated from the frequency of the maximum peak of the semicircle. Correspondingly, the characteristic frequency shown in Bode phase plots is shifted to a higher value for the MPTS/P25 sample, suggesting the electron lifetime is shortened, as tabulated in Table 1. This shift can be ascribed to a difference in the local I_3^- concentration, and the lower transport resistance and lifetime are attributed to the high combination rate of the MPTS/P25 sample, which has higher efficiency. Interestingly, a similar behavior was reported by Xia et al. [22] using nanoparticles and aggregate photoelectrodes. They reasoned that their finding was the result of easier electron transfers within the photoelectrodes and easier subsequent charge transfers at the photoelectrode/FTO interface, which are beneficial for both electron generation and transport. Therefore, our results may be attributed

Table 1

Impedance data analysis through fitting the curves with appropriate equivalent circuit.

	R_1	R_2	R_3	τ
P25/MPTS	14.28	17.1	90.26	0.50
P25	13.11	16.67	106.6	0.79

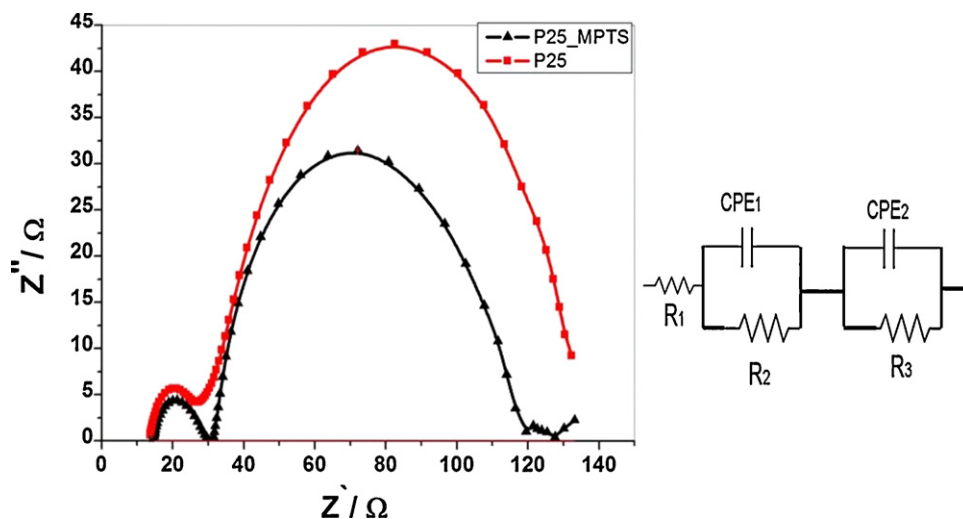


Fig. 5. EIS spectra showing Nyquist plots of the MPTS/P25 and bare P25 DSC. The inset shows the equivalent circuit.

to the increase in pore size for the MPTS/P25 sample and, thus, the increases in the dye adsorption and penetration of the redox couples in the pores [27] where the recombination centers are close to the surface of the nanoparticles. Kang et al. [28] reported that a lower lifetime for a mesoporous structure is attributed to its larger surface area, which is proportional to the charge recombination between the injected electrons and the redox species where many defect states are induced by an increased surface area. Such defect states provide many pathways by which charge recombination can occur within the interfaces.

Other studies [29–31] have reported an increase in charge transfer resistance by suppressing the surface of the photoelectrode using ALD of specific metal oxides. This suppression enhances the open circuit voltage (see Eq. (1)) and the overall efficiency by reducing the recombination rate. Therefore, we believe that the lower charge transfer resistance for the MPTS/P25 sample is due to the mesoporous structure and its larger specific surface area [28]. Moreover, the decreased charge transfer resistance is the reason for the higher FF for the MPTS/P25 sample. In similar studies [32,33], it has been observed that a larger contact area with the dye reduces the charge transfer resistance and consequently increases the efficiency of the cell.

3.6. Performance of the DSC

The performances of the dye-sensitized solar cells fabricated using MPTS-modified TiO₂ nanoparticles and unmodified nanoparticles with AM 1.5 simulated solar lights (100 mW/cm²) were measured, and the results are shown in Fig. 6 and tabulated in Table 2. In these findings, the photocurrent density increased from 10 to 14.9 mA/cm², and the open circuit voltage increased from 628 to 698 mV when using the UV-polymerized MPTS matrix. The calculated energy conversion efficiency (η) was also nearly doubled for the MPTS-modified sample and had a superior quality compared with the unmodified sample. Additionally, the MPTS-modified sample had a filling factor of 64%, which was larger than the unmodified sample with a filling factor of 55%.

Table 2
DSC performances for unmodified and MPTS modified P25 nanoparticles.

	J_{sh} (mA/cm ²)	V_{oc} (Volt)	FF	η (%)
P25/MPTS	14.85	0.698	0.64	6.57
P25	10.05	0.62	0.55	3.38

The most crucial DSC improvement made using the MPTS sample should be attributed to its significant increase in the photocurrent density; however, a smaller contribution can also be ascribed to its enhancement of the open-circuit voltage. The reasons for the improvements to the photocurrent density may be correlated to multiple different factors, such as dye adsorbance, incident photon flux, charge injection efficiency, dye regeneration efficiency and charge collection efficiency.

The silica-modified nanoparticles exhibited a higher dye loading (Fig. 4) and larger surface roughness factor, which is 37% larger than the bare nanoparticles. These findings mean more dye adsorbed and hence higher photocurrent was injected. In addition to the increase in photocurrent, the larger surface area and larger pore volume attained by the silica-modified system assisted the immobilization of the electrolyte to be close to the dye, which led to higher dye regeneration. More specifically, the flux of the electrolyte species through the mesoporous structure of the photoanode affected the photocurrent density. For instance, Lee et al. [34] reported a similar behavior using virus-templated TiO₂ nanoparticles. In this study, the impedance components were reduced due to the generation of highly interconnected mesopores inside the electrode and due to the subsequent acceleration of the redox activity of the electrolyte. These factors yielded a decrease in the diameter of the large semicircles and an increase in photocurrent density.

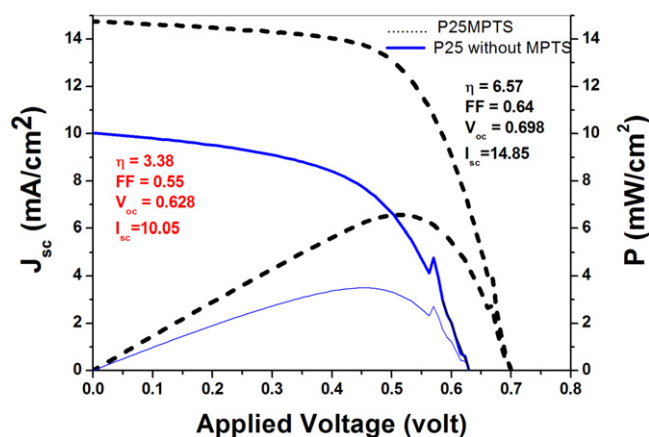


Fig. 6. Photocurrent density versus the applied voltage for modified and unmodified MPTS P25 nanoparticles DSCs under AM 1.5 at 100 mW/cm² illumination.

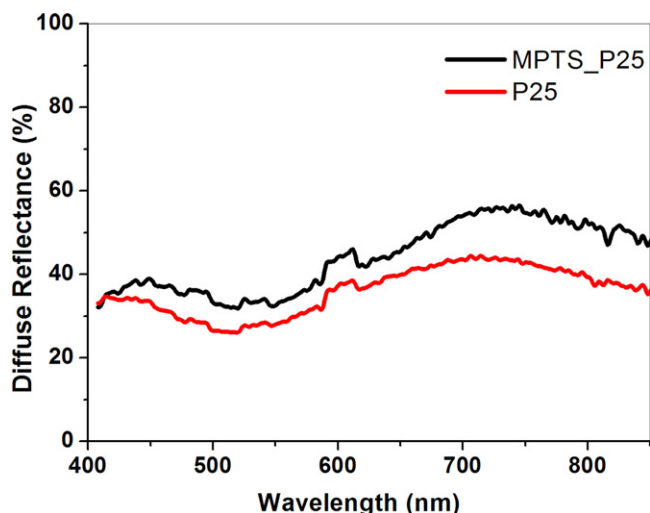


Fig. 7. Diffuse reflectance for MPTS/P25 and P25 based photoanode.

Any increase of light scattering within the photoanode layer affects the light harvesting efficiency. However, the existence of larger aggregated nanoparticles within the silica-treated sample, as exhibited in the surface morphology (Fig. 2), may extend the light path within the mesoporous photoanode and retain the surface area of the mesoporous structure [6], increasing the photon capture by the dye molecule. For example, Zhang et al. fabricated popcorn-style, dye-sensitized solar cells with porous electrodes made of submicron-sized aggregates (or popcorns) of ZnO nanocrystallites, and they demonstrated a significant enhancement in power conversion efficiency [35].

In addition to that fact, the presence of two inorganic materials (silica and TiO₂ networks), according to the proposed network in Scheme 1, with different indices of refraction is expected to alter the reflection of a light beam. Therefore, the diffuse reflectances of both layers should help us understand the light harvesting mechanism for these DSCs. It is shown in Fig. 7 that the silica-treated sample exhibits a higher diffuse reflectance than the bare P25 layer. Additionally, the largest increase in light scattering is the most obvious in the near-infrared region because of the back scattering of light within the porous structure. Wu et al. [36] also reported this higher diffuse reflectance in the long wavelength range for a double-layered shell-in-shell TiO₂ hollow sphere, which is considered as the argument of higher obtained photocurrent density. Overall, the enhanced photoconversion efficiency driven by the increased current density attributed primarily to an increased dye uptake amount, which was due to the larger surface area and optimized paths for electron transport in the DSC, the fast redox activity of the electrolyte at the working electrode interface, and the enhancement of light scattering inside the TiO₂ multiporous structure.

The proposed model illustrated in Scheme 1A indicates that the polymerization of MPTS may result in the presence of a thin Si–O–Si network covered in TiO₂ nanoparticles, which were connected and merged together to form an electrical path for the charge carriers. This coverage of the silica network may result in a shift of the flat band potential for the TiO₂ to a negative value as a consequence of the surface dipole generated at the TiO₂/silica interface [37]. However, the increase of the open circuit voltage could also be due to the band bending which can occur at the interface of the TiO₂/silica. For instance, when silica is present on the surface of TiO₂, a potential is created across the interface because the Fermi levels of both compounds attempt to equilibrate; this potential across the interface leads to band bending [38].

In our study, it is anticipated that the silica preferentially forms a suppression layer over the TiO₂ nanoparticles, which would then create an energy barrier restricting surface charge recombination and favor a higher open circuit voltage. A homogeneous distribution of oxides such as MgO, Al₂O₃, SiO₂ and Nb₂O₅ on SnO₂ and TiO₂ nanocrystallites have been reported by Palomares et al. [39], and these oxides lead to an increase in the open-circuit voltage. Similar results were also reported by depositing ultra-thin HfO and Al₂O₃ layers onto the surface of TiO₂ nanoparticles [40].

4. Conclusion

A silica-coupling agent was used successfully in dye-sensitized solar cells to modify and incorporate commercial TiO₂ (P25) nanoparticles into a mesoporous network with a high surface area and larger sensitizer surface coverage than a bare P25 sample. Another benefit to this modified DSC is that it has a higher efficiency due to its high photocurrent density. Additionally, its more compact mesoporous structure results in an increase of the electrochemical kinetics, which in turn improves the accessibility of the dye and of the electrolyte to the electrode. Overall, a light conversion efficiency of 6.5%, an open-circuit voltage (V_{OC}) of 698 mV, a short-circuit current density (J_{SC}) of 14.8 mA/cm², and a fill factor (FF) of 64% were achieved using the silica-treated mesoporous TiO₂ electrode, all of which were significantly higher values than those achieved using the bare P25 TiO₂ electrode (3.4%).

Acknowledgements

Naji Al Dahoudi thanks the Fulbright grant sponsored by the US Department of the State for his work during his visit to the Materials Science and Engineering (MSE) Department at University of Washington. This work was also supported in part by the National Science Foundation (DMR-1035196), the Boeing-Steiner Endowment, the University of Washington TGIF grant and Intel Corporation.

References

- [1] B. O'Regan, M. Graetzel, *Nature* 353 (1991) 737.
- [2] A. Hagfeldt, M. Graetzel, *Chem. Rev.* 95 (1995) 49.
- [3] M. Graetzel, *Nature* 414 (2001) 338.
- [4] K. Sayama, H. Sugihara, H. Arakawa, *Chem. Mater.* 10 (1998) 3825.
- [5] M. Graetzel, *J. Photochem. Photobiol. C: Photochem. Rev.* 4 (2003) 145.
- [6] Q. Zhang, G. Cao, *Nano Today* 6 (2011) 91.
- [7] M.K. Mazeruddin, A. Kay, I. Rodicio, R. Humphry-Baker, E. Mueller, P. Liska, N. Vlachopoulos, M. Graetzel, *J. Am. Chem. Soc.* 115 (1993) 6382.
- [8] N. Al Dahoudi, PhD Thesis, University of Saarland, Germany, 2003.
- [9] H. Byrne, W. Kostedt IV, J. Stokke, D. Mazyck, *J. Non-Cryst. Solids* 355 (2009) 525.
- [10] Sh. Pazokifard, S. Mirabedini, M. Esfandeh, M. Mohseni, Z. Ranjbar, *Surf. Interface Anal.* (2011), doi:10.1002/sia.3767.
- [11] K. Okada, A. Yoshizawa, Y. Kameshima, T. Isobe, A. Nakajima, K.J. Mackenzie, *J. Porous Mater.* 18 (2011) 345.
- [12] M. Suarez, G. Palmisano, M. Ferrer, M. Gutierrez, S. Yurdakal, V. Augugliaro, M. Pagliaro, *F. del Monte, J. Mater. Chem.* 19 (2009) 2070.
- [13] A. Fadeev, T. McCarthy, *J. Am. Chem. Soc.* 121 (1999) 12184.
- [14] A. Fadeev, T. McCarthy, *Langmuir* 15 (1999) 3759.
- [15] A. Fadeev, T. McCarthy, *Langmuir* 16 (2000) 7268.
- [16] C. González, J. Fraile, A. López-Periago, C. Domingo, *J. Colloid Interface Sci.* 338 (2009) 491.
- [17] O. Lichtenberger, J. Woltersdorf, *Mater. Chem. Phys.* 44 (1996) 222.
- [18] H. Nur, *Mater. Sci. Eng. B* 133 (2006) 49.
- [19] B. Malinowska, J. Walendziewski, D. Robert, J.V. Weber, M. Stolarski, *Appl. Catal. B: Environ.* 46 (2003) 441.
- [20] M. Kang, M. Lee, *Appl. Catal. A: Gen.* 284 (2005) 215.
- [21] K. Kakiuchi, E. Hosono, S. Fujihara, *J. Photochem. Photobiol. A: Chem.* 179 (2006) 81.
- [22] J. Xia, Q. Zhanga, K. Parka, Y. Sun, G. Cao, *Electrochim. Acta* 56 (2011) 1960.
- [23] H.-G. Jung, Y. Kang, Y. Sun, *Electrochimica Acta* 55 (2010) 4637.
- [24] Y. Guo, PhD Thesis, University of Saarland, Saarbruecken, Germany, 2002.
- [25] J. Wu, G. Chen, H. Yang, C. Ku, J. Lai, *Appl. Phys. Lett.* 90 (21) (2007) 213109.
- [26] Q. Wang, J. Moser, M. Graetzel, *J. Phys. Chem. B* 109 (2005) 14945.
- [27] C. Hsua, K. Lee, J. Huang, C. Lin, C. Lee, L. Wang, S. Tsai, K. Hu, *Electrochim. Acta* 53 (2008) 7514.

- [28] S.H. Kang, J. Kim, Y. Sung, *Electrochim. Acta* 52 (2007) 5242.
- [29] K. Park, Q. Zhang, B. Garcia, X. Zhou, Y. Ha Jeong, G. Cao, *Adv. Mater.* 22 (2010) 2329.
- [30] V. Ganapathy¹, B. Karunakaran¹, Shi-Woo Rhee, J. Power Sources 195 (2010) 5138.
- [31] M.-H. Kim, Y.-U. Kwon, *J. Phys. Chem. C* 113 (2009) 17176.
- [32] C. Lee, L. Yin Lin, K. Wei Tsai, R. Vittal, K. Chuan Ho, *Journal of Power Sources* 196 (3) (2010) 1632.
- [33] K. Lee, J. Kim, H. Kim, Y. Lee, Y. Tak, *J. Korean Phys. Soc.* 54 (3) (2009) 1027.
- [34] Y. Lee, Y. Kim, J. Lee, J. Park, N. Park, W. Choe, M. Ko, P. Yoo, *Adv. Funct. Mater.* 21 (6) (2011) 1160.
- [35] Q.F. Zhang, C. Dandeneau, X.Y. Zhou, G. Cao, *Adv. Mater.* 21 (2009) 4087.
- [36] X. Wu, G. Lu, L. Wang, *Energy Environ. Sci.* 4 (2011) 3565.
- [37] Y. Diamant, S. Chen, O. Melamed, A. Zaban, *J. Phys. Chem. B* 107 (2003) 1977.
- [38] H. Jafry, M. Liga, Q. Li, A. Barron, *Environ. Sci. Technol.* 45 (2011) 1563.
- [39] E. Palomares, J. Clifford, S. Haque, T. Lutz, J. Durrant, *J. Am. Chem. Soc.* 125 (2003) 475.
- [40] M. Shanmugam, M. Baroughi, D. Galipeau, *Thin Solid Films* 518 (2010) 2678.